STRUCTURAL BIOLOGY

**Volume 79 (2023)**

**Supporting information for article:**

# Structural and binding studies of a new chitin-active AA10 lytic polysaccharide monooxygenase from the marine bacterium *Vibrio campbellii*

**Yong Zhou, Suttipong Wannapaiboon, Methinee Prongjit, Soraya Pornsuwan, Jeerus Sucharitakul, Nuntaporn Kamonsutthipaijit, Robert C. Robinson and Wipa Suginta**

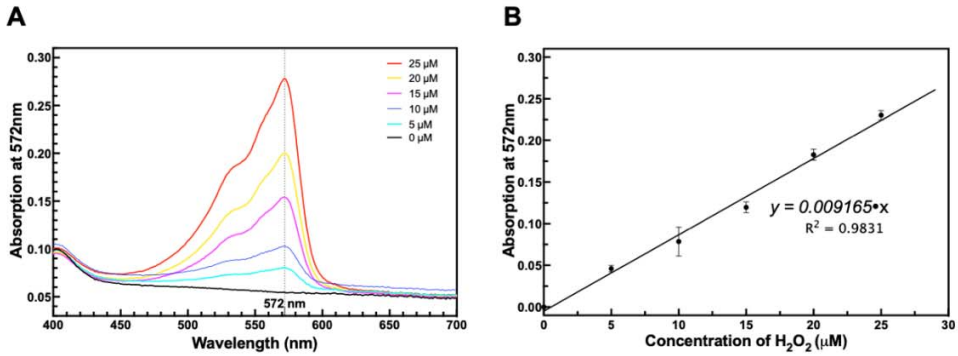


**Figure S1** Absorption spectra of oxidized Amplex™ Red. (A) Various concentrations of $H_2O_2$ were coupled to Amplex™ Red oxidation with horseradish peroxidase in the peroxide/peroxidase assay (**See Text**). The oxidized product (resorufin) showed maximal absorption at 572 nm. (B) A linear curve fit of the peak absorption value ($A_{572}$) *vs.* $H_2O_2$ concentration.

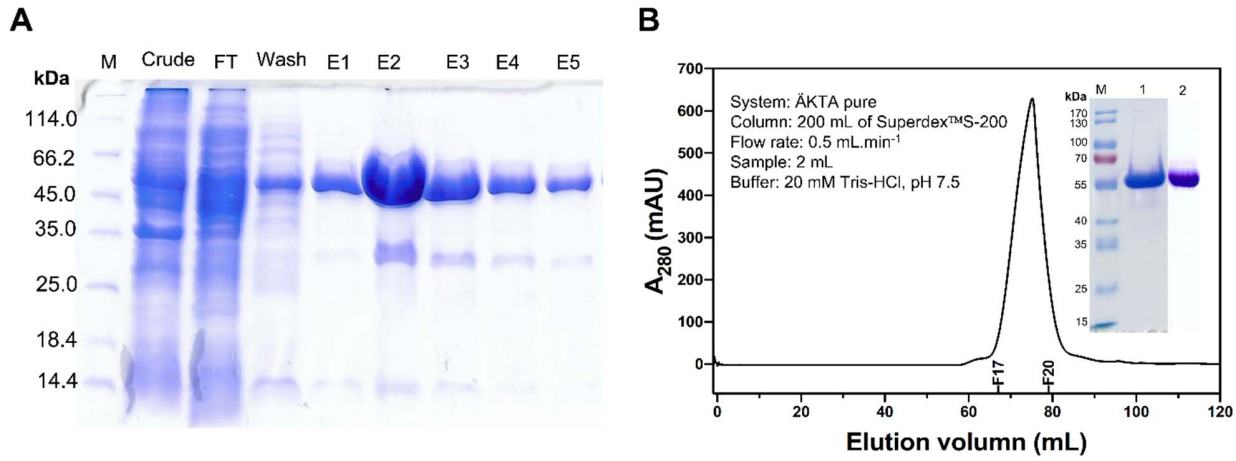


**Figure S2** Heterologous expression and purification of the recombinant *Vh*LPMO10A. *Vh*LPMO10A was expressed in *E. coli* BL21 (DE3) and purified to homogeneity as described in Materials and Methods. (A) SDS-PAGE analysis of the protein after affinity purification. Lanes: Crude, LPMO-containing supernatant after removal of cell debris; FT, flow-through collected after protein loading; Wash, fraction washed with 20 mM imidazole; E1-5, fractions obtained on elution with 150 mM imidazole. (B) A representative gel filtration profile of copper-bound *Vh*LPMO10A. Pooled fractions F17-F20 from $A_{280}$ peak were analyzed by SDS-PAGE. Both protein samples migrated to the expected molecular weight of *Vh*LPMO10A (51,142 Da). Lanes (inset): M, standard protein marker; 1, $Cu^{2+}$-saturated *Vh*LPMO10A; 2, apo-*Vh*LPMO10A.

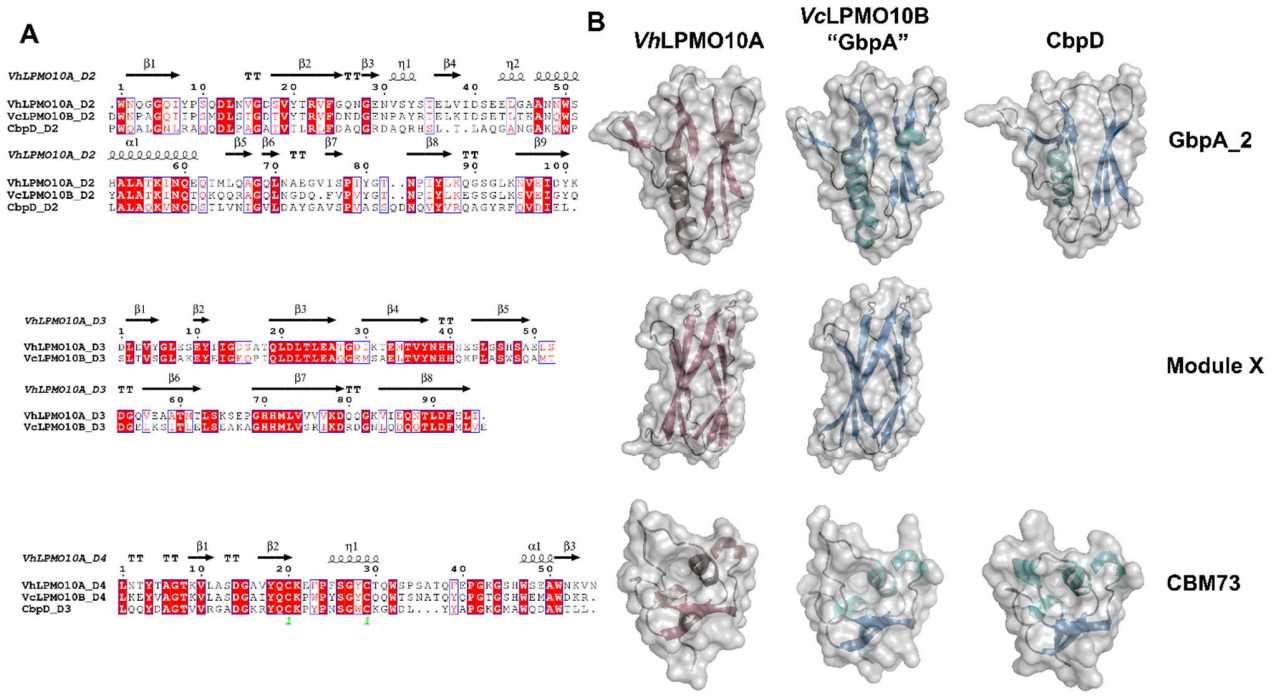


**Figure S3** Sequence and structural analysis of GbpA_2, Module X and CBM73 domains of *Vh*LPMO10A. (A) Sequence alignments of GbpA_2, Module X and CBM73 domains of *Vh*LPMO10A with the known structural homologs from *Vc*LPMO10B (GbpA) and CbpD, respectively. Secondary structure elements are indicated as follows: α, alpha helix; η, 310 helixes; β, beta-strand; T, turn. The pair of cysteines forming a disulfide bridge is labelled with green numbers. The sequence alignment was performed by MUSCLE and the secondary structure elements were constructed by ESPript v.3.0. (B) Structural comparisons of GbpA_2, Module X and CBM73 domains of *Vh*LPMO10A with *Vc*LPMO10B (GbpA) (PDB id: 2xwx) and CbpD (PDB id: 7sqx), respectively. Notably, the structures of CBM73 domain from *Vc*LPMO10B (GbpA) and CbpD were predicted by AlphaFold2 since this domain is missing in their crystal structures.

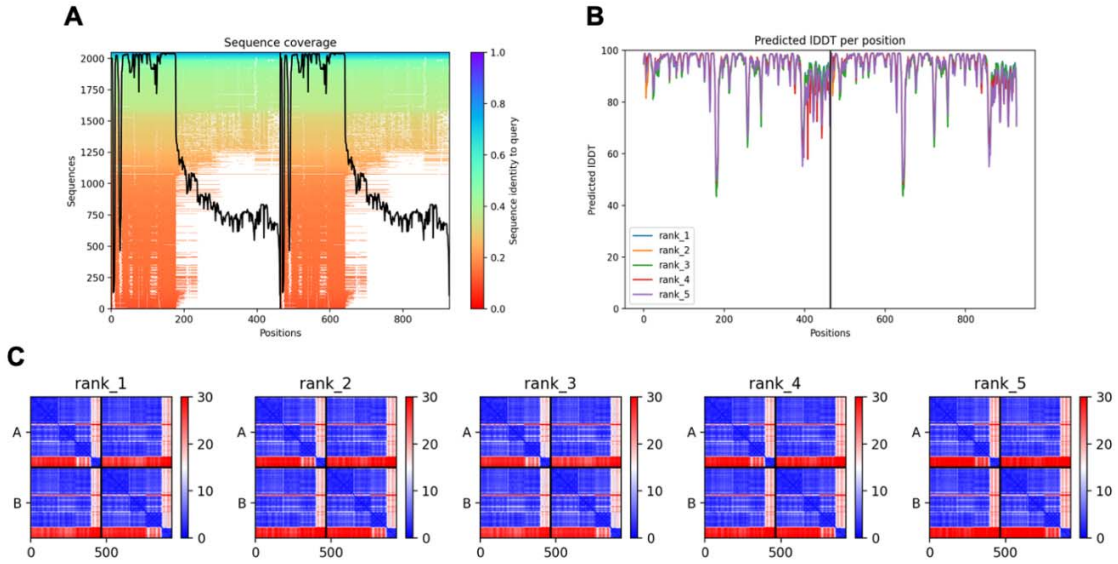


**Figure S4** The confidence output files of the *Vh*LPMO10A dimer predicted by the AlphaFold2 online tool**.** (A) Sequence coverage of *Vh*LPMO10A *vs.* amino acid position. (B) The predicted local-distance difference test (lDDT) and (C) predicted aligned error (PAE) with five predicted models in which PAE values between the first 3 domains chains are low (blue), indicating a confident prediction of dimerization between these 3 domains. The C-terminal domain shows high (red) PAE values for the positioning relative to the first 3 domains and relative to the dimer. This indicates that the relative position of the C-terminal domain is likely to be flexible.

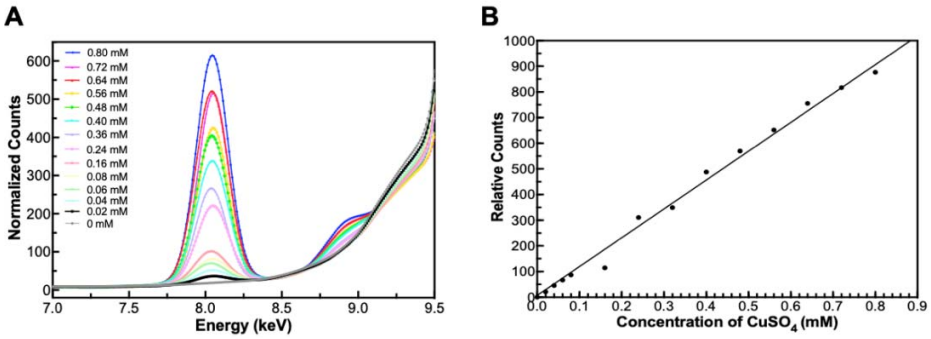


**Figure S5** Energy-dispersive XRF standard curve of $CuSO_4$**.** (A) XRF spectra of $CuSO_4$ from 0 to 0.8 mM scanned using a monochromatic X-ray beam with an energy of 10 keV for excitation and an acquisition time of 300 s. (B) A linear XRF standard curve fit of the relative counts *vs.* $H_2O_2$ concentration at the characteristic Cu(II) peak (K-alpha, 8.045 keV). Samples of 500 $\mu$L, containing various concentrations of $CuSO_4$ in 20 mM Tris-HCl, pH 7.5, were placed in plastic bags (20mm × 30mm) and were exposed to the X-ray beam only during the measurements, to avoid radiation damage. The characteristic Cu(II) K-alpha XRF signal was monitored. The current potential, ICR (kcps), dead-time and counts were recorded by ProsPect software.

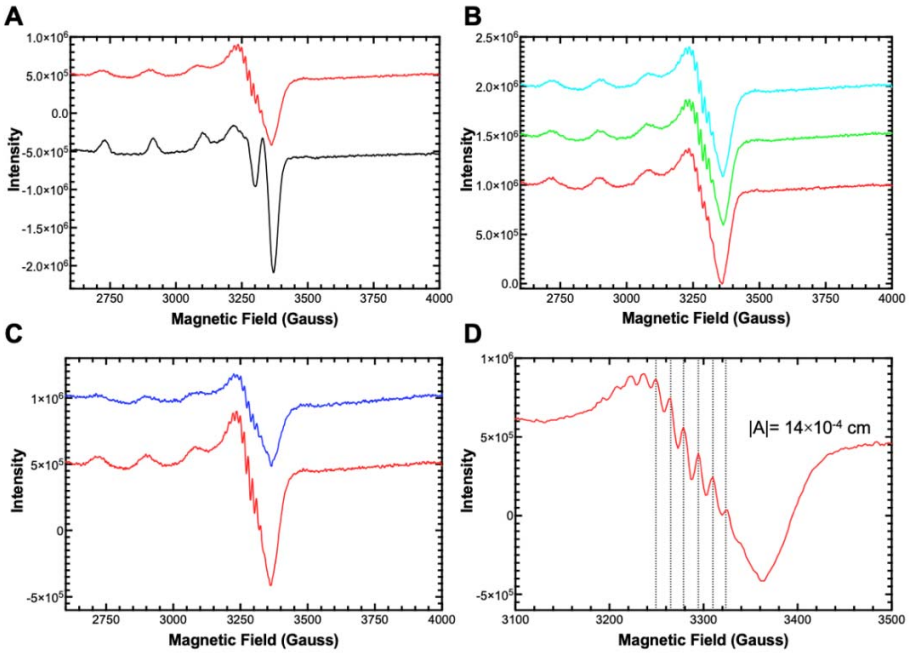


**Figure S6** Copper binding studies by EPR spectroscopy. (A) EPR spectra of copper-saturated *Vh*LPMO10A-Cu(II) (red line) compared to a control containing only free Cu(II) in the same buffer (black line). (B) EPR spectra of *Vh*LPMO10A incubated with various ratios of Cu(II) to *Vh*LPMO10A: 1:1 (red line), 1:5 (green line), and 1:10 (cyan line), respectively. (C) EPR spectra of Cu(II)-loaded *Vh*LPMO10A (red line) in the absence (red line) or presence (blue line) of ascorbic acid. (D) EPR spectrum of Cu(II)-loaded *Vh*LPMO10A showing the splitting constant of |A|= 14x10$^{-4}$ cm. All EPR experiments were performed under aerobic conditions. Samples were in 20 mM Tris-HCl, pH 7.0, and spectra were recorded at 125 K with a 2mW microwave power and a 2 Gauss modulation amplitude. The data are based on a single experiment (n = 1).

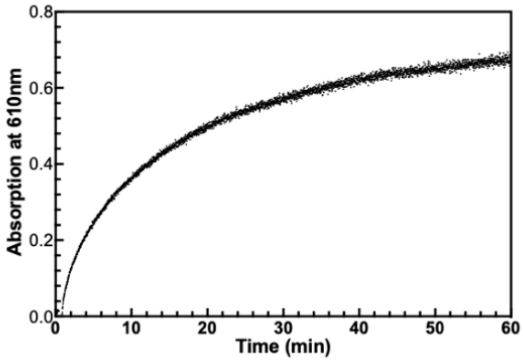


**Figure S7** The adsorption spectra of cell potential ($E^o$) analysis for the *Vh*LPMO10A-$Cu^{2+}$/*Vh*LPMO10A-$Cu^{+}$ redox couple. $Cu^{2+}$-saturated *Vh*LPMO10A (50 $\mu$L,140 $\mu$M) was incubated at room temperature (25°C) with 50 $\mu$l of an oxygen-free *N, N, N', N'*-tetramethyl-1,4-phenylenediamine ($TMP_{red}$) in its reduced form (600 $\mu$M or 400 $\mu$M) in oxygen-free 20 mM tris buffer, pH 7.5. The solutions were made oxygen-free by bubbling $N_2$ gas through the buffer for 1 h prior to the addition of $TMP_{red}$ and concentrated LPMO solution. The reaction took place in a UV cuvette (Eppendorf) sealed by parafilm and placed in an Agilent Cary Series UV-Vis spectrophotometer. TMP radical cation ($TMP_{ox}$), which was the product of the reaction, was monitored continuously by measuring absorbance at 610 nm until the signal became stable.

| | |
|---|---|
| **I)** | |
| $TMP_{red}$ + *Vh*LPMO10A-$Cu^{2+}$ ⇌ $TMP_{ox}$ + *Vh*LPMO10A-$Cu^{+}$ | $K$ = 0.7, $E°$ = -9.5 mV |
| $TMP_{ox}$ + $e^-$ →$TMP_{red}$ | $E°$ = 273.0 mV |
| *Vh*LPMO10A-$Cu^{2+}$ + $e^-$ → *Vh*LPMO10A-$Cu^{+}$ | $E°$ = 263.5 mV |
| **II)** | |
| $Cu^{2+}$ +e- →$Cu^{+}$ | $E°$ = 160.0 mV |
| *Vh*LPMO10A-$Cu^{+}$ → *Vh*LPMO10A-$Cu^{2+}$ + $e^-$ | $E°$= -263.5 mV |
| $Cu^{2+}$ + *Vh*LPMO10A-$Cu^{+}$ ⇌ $Cu^{+}$ + *Vh*LPMO10A-$Cu^{2+}$ | $E°$ = –103.5 mV, $\Delta Gr°$ = 2.4 kcal/mol |
| **III)** | |
| $Cu^{2+}$ + *Vh*LPMO10A-$Cu^{+}$ ⇌ $Cu^{+}$ + *Vh*LPMO10A-$Cu^{2+}$ | $E°$ = –103.5 mV, $\Delta Gr°$ = 2.4 kcal/mol |
| *Vh*LPMO10A-$Cu^{2+}$ ⇌ *Vh*LPMO10A + $Cu^{2+}$ | $K_d$ = 110 nM, $\Delta Gr°$ = 9.5 kcal/mol |
| *Vh*LPMO10A-$Cu^{+}$ ⇌ *Vh*LPMO10A + $Cu^{+}$ | $\Delta Gr°$ = 11.9 kcal/mol, $K_d$ = 1.9 nM |

**Figure S8** Calculation of the *Vh*LPMO10A-$Cu^{1+}$ dissociation constant. The $K_d$ of *Vh*LPMO10A binding to $Cu^{1+}$ can be calculated by combining three thermodynamic parameters. First, the cell potential ($E°$) of *Vh*LPMO10A-$Cu^{2+}$/ *Vh*LPMO10A-$Cu^{1+}$ was derived experimentally by determining the equilibrium constant for the electron transfer reaction between the mediator $TMP_{red/ox}$ and *Vh*LPMO10A-$Cu^{2+/1+}$ (reaction scheme I). The cell potential was obtained from the equilibrium constant using the relationship $RT\ln K = nFE°$. Second, the $E°$ from thermodynamic relation I was combined with the known $E°$ for reduction of $Cu^{2+}$ in aqueous conditions to yield the free energy change ($\Delta G_r°$) for the reduction of aqueous $Cu^{2+}$ by *Vh*LPMO10A-$Cu^{1+}$ (reaction scheme II) using the relationship $\Delta G_r° = -nFE°$. Third, combining the $\Delta G_r°$ measured for dissociation of *Vh*LPMO10A-$Cu^{2+}$ (**Fig. 5** and **Table 2**) with $\Delta G_r°$ deduced from the electron transfer reaction between aqueous $Cu^{2+}$ and *Vh*LPMO10A-$Cu^{1+}$, the dissociation of *Vh*LPMO10A-$Cu^{1+}$ can be calculated (reaction scheme III) using the relationship $\Delta G_r° = RT\ln K_d$.

**Table S1** Fifteen bacterial AA10 LPMOs from with name of orgnanisms used for multiple sequence alignment. GenBank ID and Uniprot ID, which correspond to the names, are shown in **Fig. 1**.

| **Name** | **Organism** | **GenBank ID** | **Uniprot ID** |
|---|---|---|---|
| *Ba*LPMO10A | *Bacillus amyloliquefaciens* | CBI42985.1 | E1UUV3 |
| *Bc*LPMO10A | *Bacillus cereus* | WP_001065157.1 | Q81CG6 |
| *Bl*LPMO10A | *Bacillus licheniformis* | AAU39477.1 | D0EW67 |
| *Bt*LPMO10A | *Bacillus thuringiensis* | AJP62637.1 | A0A0C5K362 |
| *Cj*LPMO10A | *Cellvibrio japonicus* | AAO80225.1 | Q838S1 |
| *Ef*LPMO10A | *Enterococcus faecalis* | AAO80225.1 | Q838S1 |
| *Jd*LPMO10A | *Jonesia denitrificans* | ACV09037.1 | C7R4I0 |
| *Lm*LPMO10A | *Listeria monocytogenes* | CAD00545.1 | Q8Y4H4 |
| *Pl*LPMO10A | *Photorhabdus Luminescens* | CAE14645.1 | Q7N4I5 |
| *Sam*LPMO10B | *Streptomyces ambofaciens* | CAJ89556.1 | A3KIM2 |
| *Sg*LPMO10F | *Streptomyces griseus* | BAG23684.1 | B1VN59 |
| *Sli*LPMO10E | *Streptomyces lividans* | EOY47895.1 | A0A7U9DRA2 |
| *Sm*LPMO10A (CBP21) | *Serratia marcescens* | AAU88202.1 | O83009 |
| *Vc*LPMO10B (GbpA) | *Vibrio cholerae* | AAF96709.1 | Q9KLD5 |
| *Vh*LPMO10A | *Vibrio harveyi* | WP_011999056.1 | A7N3J0 |

**Table S2** MALDI-TOF-MS analysis of the representative oxidized products ($DP2_{ox}$ and $DP8_{ox)}$ obtained from the cleavage of shrimp chitin by *Vh*LPMO10A.

| | Oxidized product | Theoretical MW | Detected MW |
|---|---|---|---|
| DP2 | $DP2_{Ox\text{-}lac} + Na^+$ | 444.3652 | 444.967 |
| | $DP2_{red} + Na^+$ | 446.3810 | 447.026 |
| | $DP2_{Ox\text{-}al} + Na^+$ | 462.3804 | 462.999 |
| | $DP2_{Ox\text{-}al} + K^+$ | 478.4890 | 478.643 |
| | $DP2_{Ox\text{-}al} + 2Na^+\text{-}H^+$ | 484.3622 | 484.836 |
| | $DP2_{Ox\text{-}al} + Na^+ + K^+\text{-}H^+$ | 500.4708 | 501.155 |
| DP3 | $DP3_{Ox\text{-}lac} + Na^+$ | 647.5572 | 648.111 |
| | $DP3_{red} + Na^+$ | 649.5730 | 650.064 |
| | $DP3_{Ox\text{-}al} + Na^+$ | 665.5724 | 666.068 |
| | $DP3_{Ox\text{-}al} + K^+$ | 681.6810 | 680.085 |
| | $DP3_{Ox\text{-}al} + 2Na^+\text{-}H^+$ | 687.5542 | 688.016 |
| | $DP3_{Ox\text{-}al} + Na^+ + K^+\text{-}H^+$ | 703.6628 | 703.555 |
| DP4 | $DP4_{Ox\text{-}lac} + Na^+$ | 850.7492 | 851.150 |
| | $DP4_{red} + Na^+$ | 852.7650 | 853.084 |
| | $DP4_{Ox\text{-}al} + Na^+$ | 868.7644 | 869.151 |
| | $DP4_{Ox\text{-}al} + K^+$ | 884.8730 | 885.058 |
| | $DP4_{Ox\text{-}al} + 2Na^+\text{-}H^+$ | 890.7462 | 891.086 |
| | $DP4_{Ox\text{-}al} + Na^+ + K^+\text{-}H^+$ | 906.8548 | 907.192 |
| DP5 | $DP5_{Ox\text{-}lac} + Na^+$ | 1053.9412 | 1054.154 |
| | $DP5_{red} + Na^+$ | 1055.9570 | 1056.177 |
| | $DP5_{Ox\text{-}al} + Na^+$ | 1071.9564 | 1072.227 |
| | $DP5_{Ox\text{-}al} + K^+$ | 1088.0650 | 1088.629 |
| | $DP5_{Ox\text{-}al} + 2Na^+\text{-}H^+$ | 1093.9382 | 1094.162 |
| | $DP5_{Ox\text{-}al} + Na^+ + K^+\text{-}H^+$ | 1110.0468 | 1100.057 |
| DP6 | $DP6_{Ox\text{-}lac} + Na^+$ | 1257.1332 | 1257.375 |
| | $DP6_{red} + Na^+$ | 1259.1490 | 1259.288 |
| | $DP6_{Ox\text{-}al} + Na^+$ | 1275.1484 | 1275.320 |
| | $DP6_{Ox\text{-}al} + K^+$ | 1291.2570 | 1291.705 |
| | $DP6_{Ox\text{-}al} + 2Na^+\text{-}H^+$ | 1297.1302 | 1297.357 |
| | $DP6_{Ox\text{-}al} + Na^+ + K^+\text{-}H^+$ | 1313.2388 | 1313.377 |
| DP7 | $DP7_{Ox\text{-}lac} + Na^+$ | 1460.3252 | 1460.407 |
| | $DP7_{red} + Na^+$ | 1462.3410 | 1462.410 |
| | $DP7_{Ox\text{-}al} + Na^+$ | 1478.3404 | 1478.481 |
| | $DP7_{Ox\text{-}al} + K^+$ | 1494.4490 | 1494.506 |
| | $DP7_{Ox\text{-}al} + 2Na^+\text{-}H^+$ | 1500.3222 | 1500.454 |
| | $DP7_{Ox\text{-}al} + Na^+ + K^+\text{-}H^+$ | 1516.4308 | 1516.734 |
| DP8 | $DP8_{Ox\text{-}lac} + Na^+$ | 1663.5172 | 1663.668 |
| | $DP8_{red} + Na^+$ | 1665.5330 | 1665.664 |
| | $DP8_{Ox\text{-}al} + Na^+$ | 1681.5324 | 1681.817 |
| | $DP8_{Ox\text{-}al} + K^+$ | 1697.6410 | 1698.049 |
| | $DP8_{Ox\text{-}al} + 2Na^+\text{-}H^+$ | 1703.5142 | 1703.957 |
| | $DP8_{Ox\text{-}al} + Na^+ + K^+\text{-}H^+$ | 1719.6228 | 1719.716 |